*Materials Transactions*, Vol. 42, No. 9 (2001) pp. 1858 to 1861


# Microstructures and the Magnetic Properties of $Fe_3B/(Nd, Dy)_2Fe_{14}B$ Nanocomposite Microalloyed with Cu and Zr *

Kagehisa Kajiwara[1], Kazuhiro Hono[1,2] and Satoshi Hirosawa[3]

[1]*Graduate School of Pure and Applied Sciences, The University of Tsukuba, Tsukuba 305-8577, Japan*
[2]*National Institute for Materials Science, Tsukuba 305-0047, Japan*
[3]*Sumitomo Special Metals Co., Ltd., Osaka 618-0013, Japan*

The effect of Zr and Cu addition to a $Nd_{3.4}Dy_1Fe_{72.3}B_{18.5}Cr_{2.4}Co_{2.4}$ alloy on the microstructure and the magnetic properties of $Fe_3B/Nd_2Fe_{14}B$ nanocomposite has been investigated by a three-dimensional atom probe (3DAP) and transmission electron microscopy (TEM). Addition of a small amount of Zr and/or Cu is effective in improving the hard magnetic properties of the base alloy. Cu atoms form clusters in the early stage of crystallization, and Zr atoms are segregated at the interfaces of $Fe_3B/Nd_2Fe_{14}B$ being rejected from the $Fe_3B$ soft magnetic phase on the optimal heat-treated condition. This causes refining the nanocomposite microstructure, resulting in improved hard magnetic properties compared to those of the base alloy.

(Received April 25, 2001; Accepted June 12, 2001)

***Keywords***: *nanocomposite magnet, hard magnetic property, melt spinning, transmission electron microscopy, atom probe*

## 1. Introduction

Since the magnetic properties of exchange coupled $Fe_3B/Nd_2Fe_{14}B$ type nanocomposite permanent magnet sensitively change depending on the grain size of soft and hard magnetic phases, many investigations have been carried out on the microstructural control by microalloying.[1–5] For example, Ping *et al.*[6] reported that micro-alloyed elements such as Cu and Nb are effective in refining the nanocomposite microstructure of $Nd_{4.5}Fe_{77}B_{18.5}$ alloy, thereby improving the hard magnetic properties. It is well known that the magnetocrystalline anisotropy, $K_u$, of the $Nd_2Fe_{14}B$ phase can be improved by replacing Nd with a heavy rare earth element such as Tb and Dy.[7] However, this does not necessarily leads to increased coercivity in the nanocomposite magnet materials, because the grain size becomes larger as a result of increased crystallization temperature. In exchange-coupled spring magnets, both remanence and $(BH)_{max}$ increase as the mean grain size decreases because stronger exchange-coupling is expected from smaller grains. On the other hand, due to the competing effect of the exchange coupling between the soft and the hard magnetic grains and that between the hard magnetic grains, coercivity is expected to decrease when the mean grain size becomes smaller than some critical value ($\sim 20$ nm).[8] It is known that the crystallization temperatures of both $Fe_3B$ and $Nd_2Fe_{14}B$ can be reduced by a small addition of Cu, since the Cu clusters that form prior to the crystallization reaction catalyze the heterogeneous nucleation of the $Fe_3B$ phase.[6] Zr addition, on the other hand, increases these crystallization temperatures, similar to Nb addition, but it appears to be effective in increasing coercivity.[9] This study aimed at understanding the role of Zr in improving the hard magnetic properties of $Fe_3B/Nd_2Fe_{14}B$ nanocomposite magnets by characterizing the microstructural features by transmission electron microscopy (TEM) and three-dimensional atom probe (3DAP).

*This Paper was Presented at the Spring Meeting of the Japan Institute of Metals, held in Narashino, on March 30, 2001.

## 2. Experimental Procedure

Amorphous ribbons with nominal compositions of $Nd_{3.4}Dy_1Fe_{72.3}B_{18.5}Cr_{2.4}Co_{2.4}$, $Nd_{3.4}Dy_1Fe_{71.9}B_{18.5}Cr_{2.4}Co_{2.4}Cu_{0.4}$, $Nd_{3.4}Dy_1Fe_{72}B_{18.5}Cr_{2.4}Co_{2.4}Zr_{0.3}$, and $Nd_{3.4}Dy_1Fe_{71.7}B_{18.5}Cr_{2.4}Co_{2.4}Cu_{0.4}Zr_{0.2}$, in addition to a base alloy composition of $Nd_{4.5}Fe_{73}B_{18.5}Cr_2Co_2$, were prepared by the single roller melt-spinning technique under an argon atmosphere at a wheel surface velocity of 7 to 20 m/s. The amorphous ribbons were isothermally heat-treated at various temperatures between 873 K and 973 K for 6 min in an argon atmosphere. Magnetic properties of these heat-treated samples were measured with a vibrating sample magnetometer (VSM) at room temperature. The crystallization behavior was investigated using a differential scanning calorimetry (DSC) at a heating rate of 20 K/min. The microstructures were characterized by a Philips CM200 transmission electron microscope (TEM) and a locally built energy compensated three-dimensional atom probe equipped with the CAMECA optical tomographic atom probe detection system.[10]

## 3. Results

The magnetic properties of the melt-spun ribbons after optimal heat treatments are summarized in Table 1. Although the coercivity increases as a result of 1 at% Dy addition to the base alloy, the remanence and $(BH)_{max}$ of Dy-containing alloys are lower than those of the base alloy. Coercivity further increases by microalloying Cu and/or Zr.

Figure 1 shows DSC traces of the as-quenched amorphous ribbons measured at a heating rate of 20 K/min. All samples show two exothermic peaks, suggesting that the crystallization from amorphous to $Fe_3B/Nd_2Fe_{14}B$ nanocomposite occurs in two stages. By TEM observation (not shown), we have confirmed that the first peak corresponds to the primary crystallization of a soft magnetic $Fe_3B$ phase from the as-melt-spun amorphous alloy and the second peak corre-

Table 1 Magnetic properties of $Fe_3B/Nd_2Fe_{14}B$ nanocomposite magnets micro-alloyed with Dy, Cu and Zr.

| Composition (at%) | $B_r$ (T) | $H_{cj}$ (kA/m) | $(BH)_{max}$ (kJ/m$^3$) |
|---|---|---|---|
| $Nd_{4.5}Fe_{73}B_{18.5}Cr_2Co_2$ | 1.05 | 378 | 108 |
| $Nd_{3.4}Dy_1Fe_{72.3}B_{18.5}Cr_{2.4}Co_{2.4}$ | 0.976 | 398 | 87 |
| $Nd_{3.4}Dy_1Fe_{71.9}B_{18.5}Cr_{2.4}Co_{2.4}Cu_{0.4}$ | 0.96 | 470 | 104 |
| $Nd_{3.4}Dy_1Fe_{72}B_{18.5}Cr_{2.4}Co_{2.4}Zr_{0.3}$ | 0.96 | 422 | 97 |
| $Nd_{3.4}Dy_1Fe_{71.7}B_{18.5}Cr_{2.4}Co_{2.4}Cu_{0.4}Zr_{0.2}$ | 0.97 | 465 | 105 |

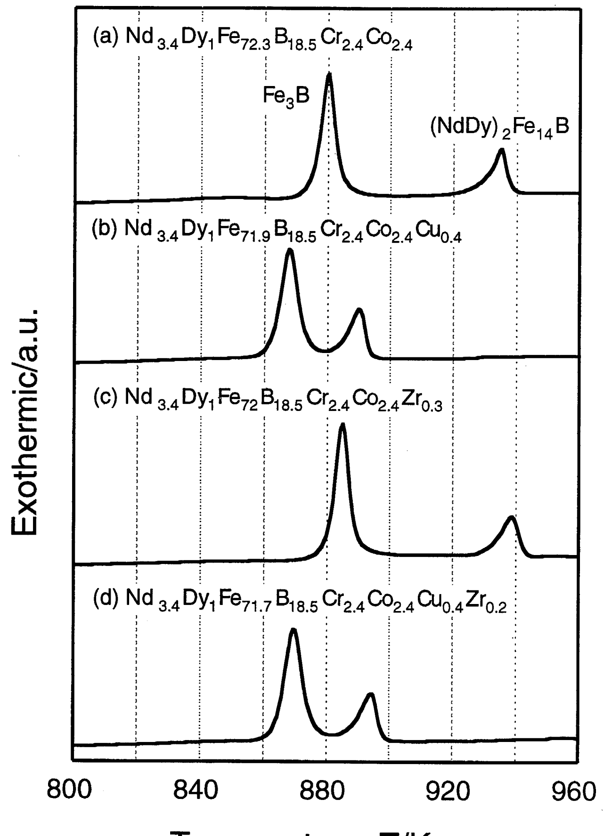


Fig. 1 DSC traces of (a) $Nd_{3.4}Dy_1Fe_{72.3}B_{18.5}Cr_{2.4}Co_{2.4}$, (b) $Nd_{3.4}D_1yFe_{71.9}B_{18.5}Cr_{2.4}Co_{2.4}Cu_{0.4}$, (c) $Nd_{3.4}Dy_1Fe_{72}B_{18.5}Cr_{2.4}Co_{2.4}Zr_{0.3}$ and (d) $Nd_{3.4}Dy_1Fe_{71.7}B_{18.5}Cr_{2.4}Co_{2.4}Cu_{0.4}Zr_{0.2}$ melt-spun ribbons scanned at a heating rate of 20 K/min.

sponds to the crystallization of the $(Nd, Dy)_2Fe_{14}B$ hard magnetic phase from the remaining amorphous matrix. Figure 1 shows that a small addition of Cu decreases the crystallization temperatures of both phases. Zr addition, on the other hand, shifts two peaks to higher temperatures. Addition of Cu to the Zr-containing alloy keeps the crystallization temperatures almost the same as those for the Cu-containing alloy. From these results, we can conclude that Cu addition reduces the crystallization temperatures, while Zr addition increases the crystallization temperatures or stabilizes the amorphous phase.

Figure 2 shows bright field TEM micrographs of all the samples with the optimum heat treatment conditions, *i.e.*, (a) $Nd_{3.4}Dy_1Fe_{72.3}B_{18.5}Cr_{2.4}Co_{2.4}$ annealed at 953 K, (b)

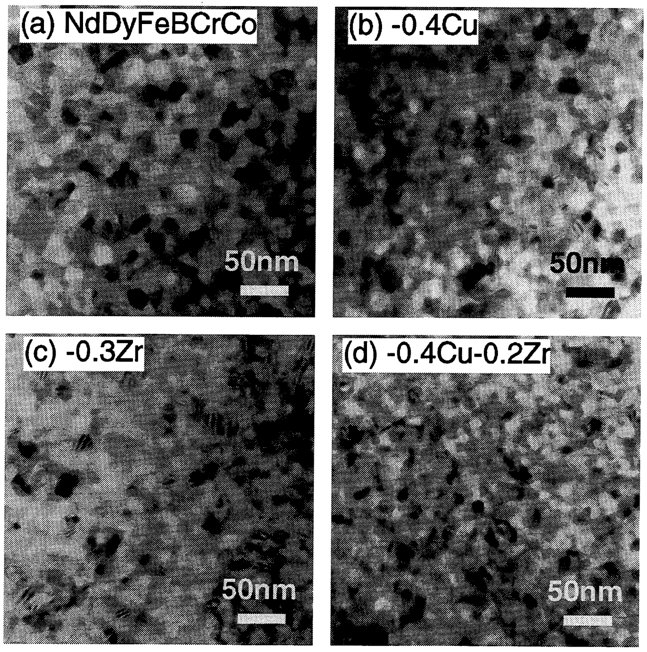


Fig. 2 TEM bright field micrographs of the optimally heat-treated of (a) $Nd_{3.4}Dy_1Fe_{72.3}B_{18.5}Cr_{2.4}Co_{2.4}$, (b) $Nd_{3.4}D_1yFe_{71.9}B_{18.5}Cr_{2.4}Co_{2.4}Cu_{0.4}$, (c) $Nd_{3.4}Dy_1Fe_{72}B_{18.5}Cr_{2.4}Co_{2.4}Zr_{0.3}$ and (d) $Nd_{3.4}Dy_1Fe_{71.7}B_{18.5}Cr_{2.4}$-$Co_{2.4}Cu_{0.4}Zr_{0.2}$.

$Nd_{3.4}Dy_1Fe_{71.9}B_{18.5}Cr_{2.4}Co_{2.4}Cu_{0.4}$ annealed at 873 K, (c) $Nd_{3.4}Dy_1Fe_{72}B_{18.5}Cr_{2.4}Co_{2.4}Zr_{0.3}$ annealed at 953 K and (d) $Nd_{3.4}Dy_1Fe_{71.7}B_{18.5}Cr_{2.4}Co_{2.4}Cu_{0.4}Zr_{0.2}$ annealed at 893 K. The grain size of the alloys containing Cu is approximately 24 nm and that of the alloy containing Zr is approximately 20 nm, which are smaller than that of the base alloy ($\sim$ 30 nm). It should be noted that the addition of only 0.2 at% of Zr has an effect to refine the crystal grain size, although a previous work reported that single addition of 2 at%Nb was not effective in refining the $Fe_3B/Nd_2Fe_{14}B$ nanocomposite microstructure.[6] The alloy containing both Cu and Zr has the smallest grain size ($\sim$ 13 nm).

Figure 3(a) shows a 3DAP elemental map of Nd and Cu in an analysis volume of approximately $11 \times 11 \times 82\,nm^3$ obtained from a $Nd_{3.4}Dy_1Fe_{71.7}B_{18.5}Cr_{2.4}Co_{2.4}Cu_{0.4}Zr_{0.2}$ alloy annealed at 893 K for 6 min. Small and large spots correspond to Nd and Cu atoms, respectively. The Nd-enriched regions correspond to the hard magnetic $(Nd, Dy)_2Fe_{14}B$ phase. Cu atoms form clusters of approximately 4 nm in the $(Nd, Dy)_2Fe_{14}B$ phase side of $Fe_3B/Nd_2Fe_{14}B$ interface. Fig. 3(b) shows elemental maps within the volume containing a Cu cluster selected from Fig. 3(a). This shows that Nd, Dy and Co are enriched with Cu atoms. The compositions of the solute elements to each phase were estimated as follow. The composition of $Fe_3B$ phase is approximately 3.6 at%Cr, 1.6 at%Co, 0.1 at%Cu and 0.1 at%Zr. The composition of $Nd_2Fe_{14}B$ phase, on the other hand, is approximately 2.1 at%Cr, 2.6 at%Co, 0.5 at%Cu and 0.2 at%Zr. Cr is preferentially partitioned in the $Fe_3B$ phase, while Co, Cu, Zr are preferentially partitioned in the $(Nd, Dy)_2Fe_{14}B$ phase. Cu forms clusters in the early stage of the crystallization, as was observed in the $Nd_{4.5}Fe_{76.8}B_{18.5}Cu_{0.2}$ alloy,[11] and these clusters triggers nucleation of the $Fe_3B$ primary crystals. In

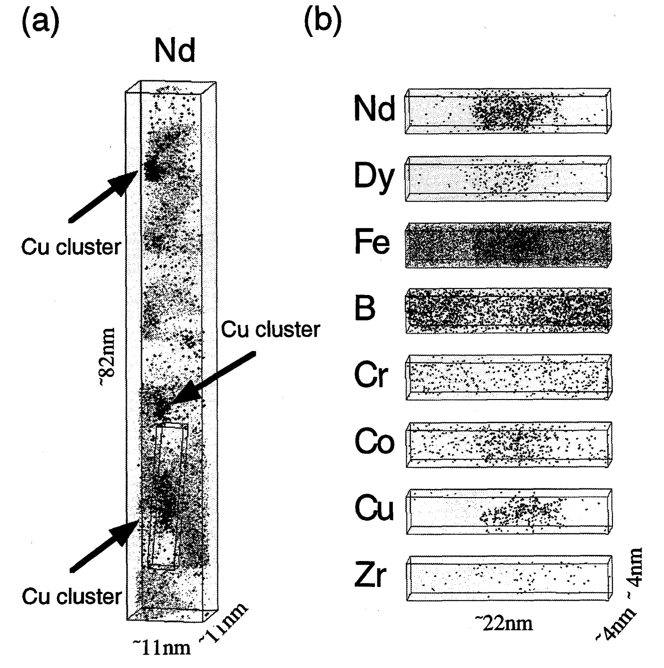


Fig. 3 EC-3DAP analysis results for $Nd_{3.4}Dy_1Fe_{71.7}B_{18.5}Cr_{2.4}Co_{2.4}Cu_{0.4}Zr_{0.2}$ nanocrystalline alloy annealed at 893 K for 6 min. (a) elemental mapping of Nd and Cu, (b) elemental mappings of solute elements.

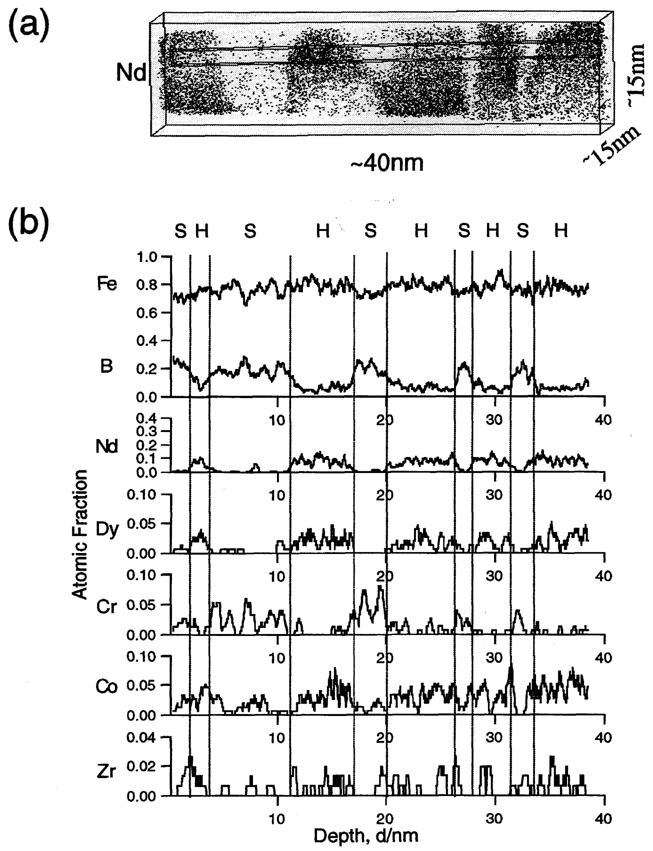


Fig. 4 3DAP analysis results for $Nd_{3.4}Dy_1Fe_{72}B_{18.5}Cr_{2.4}Co_{2.4}Zr_{0.3}$ nanocrystalline alloy annealed at 953 K for 6 min. (a) Nd elemental mapping, (b) concentration depth profiles of Fe, B, Nd, Dy, Cr, Co and Zr across interfaces. (S: soft magnetic phase, H: hard magnetic phase)

the Cu enriched region, Nd atoms were also found to be enriched as was observed in $Nd_{4.5}Fe_{77}B_{18.5}Cu_{0.2}$ alloy. Although previous 3DAP results reported that Cu clusters disappear in the final microstructure of the $Nd_{4.5}Fe_{77}B_{18.5}Cu_{0.2}$ alloy,[6] it is interesting to note that Cu enriched regions are still recognizable even in the optimized microstructure of the $Nd_{3.4}Dy_1Fe_{71.7}B_{18.5}Cr_{2.4}Co_{2.4}Cu_{0.4}Zr_{0.2}$ alloy. This may be because of the limited solubility of Cu in the $(Nd, Dy)_2Fe_{14}B$ phase. In the previous alloy, the Cu content in the alloy was only 0.2 at%Cu, while in the present alloys, 0.4 at%Cu was microalloyed. Thus, the Cu atoms insoluble in the $Nd_2Fe_{14}B$ phase would have remained as clusters in the final microstructure of the present alloys.

A Nd elemental map in an analysis volume of approximately $15 \times 15 \times 40\,nm^3$ obtained from the $Nd_{3.4}Dy_1Fe_{72}B_{18.5}Cr_{2.4}Co_{2.4}Zr_{0.3}$ alloy is shown in Fig. 4(a). Concentration profiles were calculated based on the number of atoms detected in the selected volume shown in Fig. 4(a) and the results are shown in Fig. 4(b). Preferential partitioning of Dy, Co, and Zr in the hard phase is apparent. On the other hand, Cr is enriched in the soft phase. The composition of Zr atoms was estimated to be 0.1 at% in the $Fe_3B$ phase and 0.5 at% in the $Nd_2Fe_{14}B$ phase.

Since the concentration of Zr in the alloy is only 0.2 at%, it is difficult to see the tendency of Zr partitioning because of large statistical scatter of the concentration profile. In order to observe more averaged tendency of the compositional change of Zr, integral concentration profiles of Zr at $Fe_3B/Nd_2Fe_{14}B$ interfaces are shown in Figs. 5(a) and (b), where the number of Nd and Zr atoms are plotted as functions of total number of detected atoms. Hence, the slopes of the plots correspond to the local concentration of Nd and Zr in the small volume selected across the interfaces. It can be clearly seen that Zr is slightly enriched in the $Nd_2Fe_{14}B$ phase. Furthermore, their concentration is higher at the interfaces. This indicates that Zr is segregated at the $Fe_3B/Nd_2Fe_{14}B$ interface.

In this complicated multi-component alloy, both Dy and Cr are added to increase the coercivity. Dy increases the coercivity since it increases $K_u$ by replacing Nd in the $Nd_2Fe_{14}B$ phase. Cr addition is known to increase the coercivity at the expense of remanence.[12] Cr is partitioned in the $Fe_3B$ phase as seen in Fig. 4(b), which may reduce exchange coupling among the hard grains in the nanocomposite microstructure.[13,14] Zr, on the other hand, appears to preferentially partition in the $(Nd, Dy)_2Fe_{14}B$ phase. Since Zr does not dissolve in the $Fe_3B$ phase, it is rejected from the $Fe_3B$ primary crystals during the 1st stage crystallization reaction. The Zr atoms rejected from the $Fe_3B$ particles are built up at the $Fe_3B$/amorphous interface, ending up with the segregation of Zr at the $Fe_3B/Nd_2Fe_{14}B$ interface in the final microstructure. Since Zr-containing alloys have smaller grains than the base alloy, it is concluded that this segregation of Zr at the $Fe_3B$/amorphous or $Fe_3B/Nd_2Fe_{14}B$ interfaces is the reason of the reduced grain size. In addition, this may reduce the exchange coupling through the soft phase even in the fine grain size, which may lead to increased coercivity even with the average grain size of less than 20 nm.

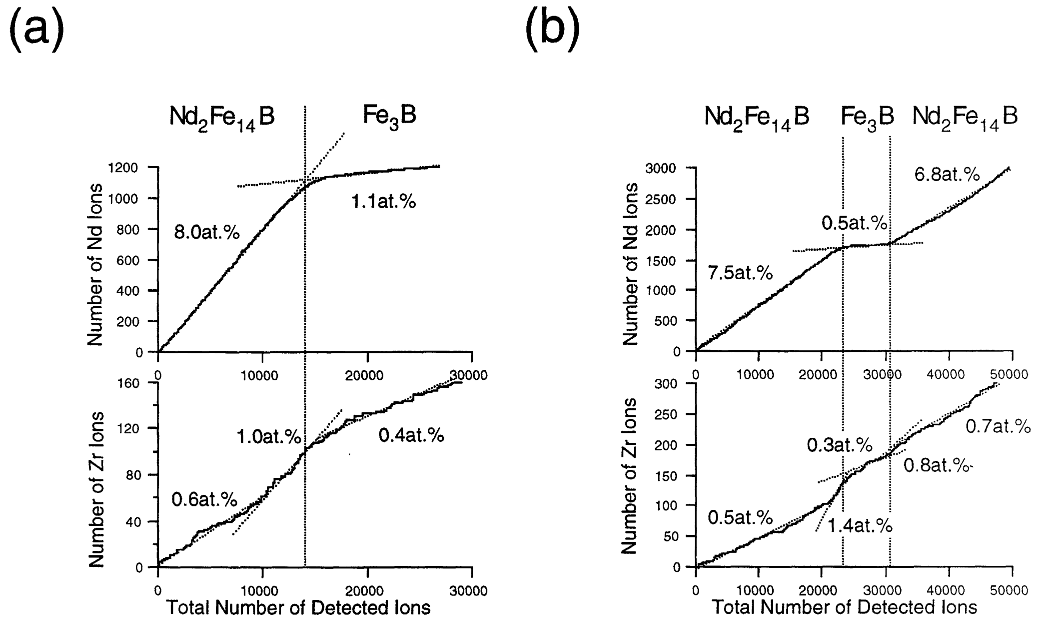


Fig. 5 Integral concentration profiles of Nd and Zr in small volume selected across interfaces for $Nd_{3.4}Dy_1Fe_{72}B_{18.5}Cr_{2.4}Co_{2.4}Zr_{0.3}$ nanocrystalline alloy annealed at 953 K for 6 min.

## 4. Conclusions

Additions of Zr and/or Cu are effective in refining the $Fe_3B/(Nd, Dy)_2Fe_{14}B$ nanocomposite microstructure of $Nd_{3.4}Dy_1Fe_{72.3}B_{18.5}Cr_{2.4}Co_{2.4}$ based alloy. Zr segregates at the $Fe_3B/Nd_2Fe_{14}B$ interface, thereby reducing the grain growth. Cu form Cu–Nd enriched clusters, which acts as heterogeneous nucleation sites for the $Fe_3B$ primary crystals. The coercivity increases as a result of Zr and/or Cu additions are attributed to the microstructure refinement.

## Acknowledgments

This work was supported by the Special Coordination Funds for Promoting Science and Technology on "Nanohetero Metallic Materials" from the Ministry of Education, Culture, Sports, Science and Technology.

## REFERENCES

1) R. Coehoorn, D. B. De Mooij, J. P. W. B. Duchateau and K. H. J. Buschow: J. Physique **49** (1988) 669.
2) R. Coehoorn, D. B. De Mooij and C. De Waard: J. Magn. Magn. Mater. **80** (1989) 101.
3) E. F. Kneller and R. Hawig: IEEE Trans. Magn. **27** (1991) 3588.
4) S. Hirosawa, H. Kanekiyo and M. Uehara: J. Appl. Phys. **73** (1993) 6488.
5) R. K. Mishra and V. Panchanathan: J. Appl. Phys. **75** (1994) 6652.
6) D. H. Ping, K. Hono, H. Kanekiyo and S. Hirosawa: Acta Mater. **47** (1999) 4641.
7) F. E. Pinkerton: J. Magn. Magn. Mater. **54–57** (1986) 579.
8) R. Fischer, T. Schrefl, H. Kronmüller and J. Fidler: J. Magn. Magn. Mater. **153** (1996) 35.
9) S. Hirosawa, T. Miyoshi, H. Kanekiyo and Y. Shigemoto: IEEE Mag. in press.
10) B. Deconihout, L. Renaud, G. Da Costa, M. Bouet, A. Bostel and D. Blavette: Ultramicroscopy **73** (1998) 253.
11) D. H. Ping, K. Hono, H. Kanekiyo and S. Hirosawa: J. Appl. Phys. **85** (1999) 2448.
12) S. Hirosawa and H. Kanekiyo: Mater. Sci. Eng. A**217/218** (1996) 367.
13) N. Sano, T. Tomida, S. Hirosawa, M. Uehara and H. Kanekiyo: Mater. Sci. Eng. A**250** (1998) 146.
14) Y. Q. Wu, D. H. Ping, B. S. Murty, H. Kanekiyo, S. Hirosawa and K. Hono: Scri. Mater. (2001) in press.